Precision Mass Measurements of Neutron-Rich Neodymium and Samarium Isotopes and Their Role in Understanding Rare-Earth Peak Formation

R. Orford,[1,2,*] N. Vassh,[3,†] J. A. Clark,[2,4] G. C. McLaughlin,[5] M. R. Mumpower,[6] G. Savard,[2,7] R. Surman,[3] A. Aprahamian,[3] F. Buchinger,[1] M. T. Burkey,[2,7] D. A. Gorelov,[2,4] T. Y. Hirsh,[2,4,8] J. W. Klimes,[2] G. E. Morgan,[2,4] A. Nystrom,[2,3] and K. S. Sharma[4]

[1]*Department of Physics, McGill University, Montréal, Québec H3A 2T8, Canada*
[2]*Physics Division, Argonne National Laboratory, Argonne, Illinois 60439, USA*
[3]*Department of Physics, University of Notre Dame, Notre Dame, Indiana 46556, USA*
[4]*Department of Physics and Astronomy, University of Manitoba, Winnipeg, Manitoba R3T 2N2, Canada*
[5]*Department of Physics, North Carolina State University, Raleigh, North Carolina 27695, USA*
[6]*Theoretical Division, Los Alamos National Laboratory, Los Alamos, New Mexico 87545, USA*
[7]*Department of Physics, University of Chicago, Chicago, Illinois 60637, USA*
[8]*Soreq NRC, Yavne 81800, Israel*

(Received 11 December 2017; revised manuscript received 2 March 2018; published 29 June 2018)

The Canadian Penning Trap mass spectrometer at the Californium Rare Isotope Breeder Upgrade (CARIBU) facility was used to measure the masses of eight neutron-rich isotopes of Nd and Sm. These measurements are the first to push into the region of nuclear masses relevant to the formation of the rare-earth abundance peak at $A \sim 165$ by the rapid neutron-capture process. We compare our results with theoretical predictions obtained from "reverse engineering" the mass surface that best reproduces the observed solar abundances in this region through a Markov chain Monte Carlo technique. Our measured masses are consistent with the reverse-engineering predictions for a neutron star merger wind scenario.

DOI: 10.1103/PhysRevLett.120.262702

The production of the elements heavier than iron in the Universe has long been associated with neutron-capture processes [1,2]. The most neutron-rich isotopes are created by rapid (r) neutron-capture nucleosynthesis [3–5] in extreme astrophysical environments. Specifics of these environments and the location of the astrophysical sites in which the r process occurs have remained open problems [6–8]. Observations of the gravitational wave event GW170817 [9] and its electromagnetic counterpart [10] have reported that neutron star mergers are a site of r-process nucleosynthesis. Still many questions remain, such as the nature of the astrophysical conditions within the merger responsible for element synthesis and whether mergers can account for all galactic r-process production. If we hope to fully understand the connection between this discovery and the origin of r-process elements, uncertainties in nuclear data, such as masses, lifetimes [11], and reaction rates [12,13], must be reduced [14–16].

A promising avenue of study involves the rare-earth element peak at $A \sim 165$, a small feature of uncertain origin between the main r-process $N = 82$ and $N = 126$ closed shell peaks. The rare-earth peak may form via a dynamical mechanism which requires the presence of a nuclear physics feature, such as a deformation maximum or a subshell closure, away from stability in the rare-earth region. This feature can present itself as a "kink" in the neutron separation energy contours in this region, which causes a pileup of material when the r-process path encounters the feature as it moves back toward stability, forming the rare-earth peak [17,18]. Many of the neutron-rich nuclei important for the operation of the dynamical mechanism are available at current generation rare isotope beam facilities, and, thus, experiments with sufficient sensitivity are well poised to shed light on r-process astrophysical conditions. Masses are particularly important, since they set the location of the r-process path and determine the neutron separation energies and Q_β values required for calculating neutron-capture rates and β-decay lifetimes. In this Letter, we report precise mass values for key neutron-rich rare-earth nuclei, $^{154,156,158-160}$Nd, and $^{162-164}$Sm, performed with the Canadian Penning Trap (CPT) mass spectrometer.

While these nuclei are of interest for rare-earth peak formation via the dynamical mechanism, it is also possible that the peak is formed by fission cycling and fission fragment distributions with just the right properties to dump material into the peak region at late times [19]; however, it is almost certain that the dynamical mechanism is the one that operates if the conditions are not neutron rich enough for fission cycling. An example of such an environment is the neutron star merger wind [20–24] in the absence of significant neutrino flavor transformation [25]. Given these astrophysical conditions, along with Duflo-Zuker masses [26], 2012 Atomic Mass Evaluation (AME2012) data [27],

and NUBASE2016 [28] experimental decay rates, we update the Markov chain Monte Carlo (MCMC) procedure, first developed in Refs. [29,30], to calculate the neutron-rich rare-earth masses which are able to reproduce the rare-earth peak of the observed solar *r*-process isotopic pattern [5,31,32]. We then compare the calculated MCMC mass values with the new CPT neodymium and samarium measurements and consider the implications for *r*-process isotope production.

The mass measurements were conducted in the low-energy experimental area of the Californium Rare Isotope Breeder Upgrade (CARIBU) facility [33] at Argonne National Laboratory using the CPT [34]. At CARIBU, neutron-rich radioactive ion beams are produced from the spontaneous fission of a $\sim$1 Ci ^{252}Cf source. Fission fragments enter a large-volume helium-filled gas catcher seated atop a 36-kV platform, where they are thermalized and transported by way of a dc electric field gradient and confining rf field before being extracted at charge states of 1+ or 2+. These fission fragments are then filtered at the desired mass-to-charge ratio (A/q) using dipole magnets at a mass resolution of $R = m/\Delta m \approx 14\,000$ before entering a helium-filled radio-frequency quadrupole (RFQ) buncher, where they accumulate for 100 ms whereupon an ejection is triggered. The energy of the resulting ion bunches is then reduced to $\sim$3.5 keV for injection into the multireflection time-of-flight (MR-TOF) mass separator [35], captured by a central *lift* electrode [36], and allowed to isochronously bounce between two electrostatic mirror electrode sets until a desired mass separation is attained. Resolving powers in excess of $R = 100\,000$ have been achieved allowing for the suppression of neighboring isobars by several orders of magnitude through the use of a Bradbury-Nielsen gate (BNG) [37] located immediately downstream of the MR-TOF. The isotope of interest is selected by the BNG and sent to the CPT system where the ion bunches are accumulated in a helium-filled linear RFQ preparation trap for injection into the CPT.

Masses were determined at the CPT using the phase-imaging ion-cyclotron-resonance (PI-ICR) technique, initially discussed by Eliseev *et al.* in Ref. [38]. This technique is inherently more efficient than the time-of-flight ion-cyclotron-resonance (TOF-ICR) method [39] which was previously used by the CPT [40,41]. Comparable mass accuracy and precision is achieved with fewer ions and shorter measurement cycles and is therefore perfectly suited for studying the most neutron-rich isotopes available at CARIBU. In PI-ICR, the locations of ions in the Penning trap are inferred by the use of a position-sensitive micro-channel plate detector. The frequency of orbital motion is determined by measuring the phase advance of ions in the Penning trap during a period of excitation-free *accumulation* time (t_{acc}). With a measurement scheme similar to "scheme 2" of Ref. [42], the cyclotron frequency (ν_c) is determined from a simultaneous measurement of the modified cyclotron frequency (ν_+) and the magnetron frequency (ν_-). A mass-independent *reference* phase is first established, in which the ions undergo purely magnetron motion for the duration of the time in the trap. Then a *final* phase is measured by exciting ν_+ motion and allowing trapped ions to accumulate a mass-dependent phase for a duration of t_{acc}. The cyclotron frequency is determined by

$$\nu_c = \frac{\phi_{\mathrm{tot}}}{2\pi t_{\mathrm{acc}}} = \frac{\phi_c + 2\pi N}{2\pi t_{\mathrm{acc}}}, \tag{1}$$

where ϕ_c is the measured angle between the reference and final phases relative to the trap center and N is the number of complete revolutions an ion undergoes in time t_{acc}.

The eight mass measurements presented here were carried out over four distinct campaigns between October 2016 and May 2017. For all measurements, the ions spend between 10 and 20 ms in the MR-TOF to achieve the desired mass resolution and necessary suppression of isobaric contamination. The total measurement cycle in the Penning trap was kept to a minimum in accordance with the half-life of the isotope of interest, and the accumulation times were individually chosen to completely resolve the desired isotope from every other trapped ion species. In order to reduce any systematic shift in the cyclotron frequency [42] due to possible imperfections in the alignment of the exit drift tube with respect to the magnetic field, these accumulation times were also chosen such that the final phase would be within $\pm 10°$ of the reference phase. To compensate for drifts in the ν_- frequency over time due to instabilities in the Penning trap trapping potentials on the order of 100 μV, reference phase measurements were routinely performed throughout each campaign. For the cases of ^{154,156,158}Nd and $^{162-164}$Sm, the production rates from CARIBU were sufficient to conduct several final phase measurements over a wide range of accumulation times between 120 and 250 ms. This gave us a well-defined understanding of the systematic uncertainties associated with the data as well as reduced statistical uncertainties. For ^{159,160}Nd, fewer data points were collected due to their smaller production rates. Depending on these rates, final phase measurements consisted of accumulating a total of 40–200 counts of the desired isotope, and in all cases the number of simultaneously trapped ions was kept to a minimum to reduce the effects of ion-ion interaction [43]. At the time of the ^{159,160}Nd measurements, only extrapolated half-lives of 500 and 300 ms from NUBASE2012 [44] were respectively available, so the total measurement cycle was reduced to 200 ms in order to detect as many ions as possible at the slight expense of ν_c precision. An example final phase measurement showing a well-resolved ^{160}Nd^{2+} is shown in Fig. 1.

To conclusively identify the circled data points in Fig. 1 as ^{160}Nd^{2+}, the detected ion rate was compared to the

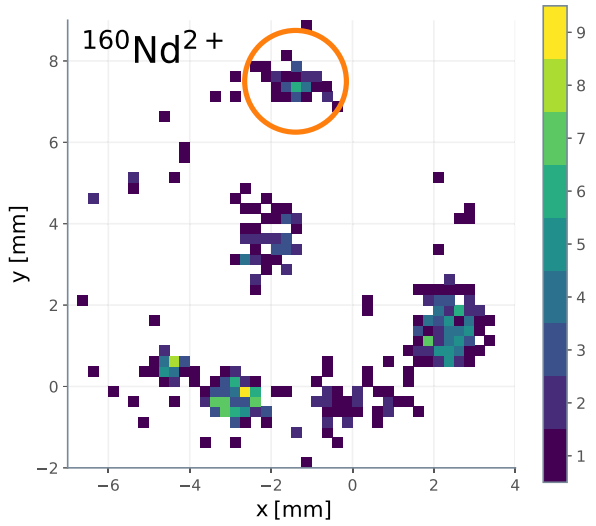

FIG. 1. A typical histogram of a final phase measurement showing the positions of ions on the detector plane. Each cluster corresponds to a different ion species present in the beam. Here we show a $t_{acc} = 55.001$ ms measurement of $^{160}Nd^{2+}$ (circled). In this example, of the 440 total ions detected in 3 hr, we observed 40 counts of $^{160}Nd^{2+}$. Also present in this spectrum are clusters of $^{160}Pm^{2+}$, three contaminant species, and some unexcited ions near the trap center.

expected ion rate based on extrapolation from fission yields in Ref. [45] relative to nearby isobars. As further proof, the measurement cycle was increased from 200 to 1700 ms, allowing for short-lived isotopes to decay in the preparation trap, and an identical final phase was measured. After accruing similar total statistics, the number of detected $^{160}Nd^{2+}$ ions had decreased consistent with having a half-life of under 1 s. All masses were calibrated within 48 hr of measurement and, with the exception of $^{159}Nd^{2+}$, were done online with isobarically pure beams of stable Kr^+ isotopes originating from trace amounts found in the ^{4}He gas inside the gas catcher. Each calibration run was done at the same ν_+ radius in the Penning trap with similar accumulation times as the target measurement under the same trapping conditions. For the case of $^{159}Nd^{2+}$, offline calibration with $^{133}Cs^+$ was required due to a vacuum failure at CARIBU. Because of the large difference in ν_c, a mass-dependent systematic uncertainty was later evaluated by measuring the masses of $^{82,84,86}Kr^+$ with respect to $^{133}Cs^+$ leading to a 7 keV correction in the final ^{159}Nd mass excess value. The new mass results are summarized in Table I. Previously, none of these masses had been measured directly, and only ^{154,156}Nd had measurements available in the literature [46,47]. In the case of ^{154}Nd, we observe a 4.8σ discrepancy from the AME2016 evaluated mass, which is not unexpected since the value is deduced from a β-endpoint energy measurement [46] using an inferred level scheme [48]. Precision mass values measured as described here are key in reducing the uncertainties within astrophysical calculations.

In the astrophysical context of a neutron star merger wind scenario, we compare the new mass measurements with predictions from our "reverse engineering" MCMC procedure. This procedure inverts the traditional approach of evaluating nuclear mass models through their r-process abundance predictions and instead uses the observational data for the rare-earth peak to find the nuclear masses required to fit this region [29,30]. We adopt conditions guided by merger wind simulations [50–52]—a hot wind with an entropy of 30 k_B/baryon, a dynamical timescale (τ) of 70 ms, and an electron fraction (Y_e) of 0.20. To perform the fit to the observational abundance data, $Y_\odot(A)$ [5,31,32], we use the Metropolis-Hastings algorithm, where the agreement between calculated abundances, $Y(A)$, and solar data, evaluated as $\chi^2 = \sum_{A=150}^{180}[Y(A) - Y_\odot(A)]^2/\Delta Y_\odot^2(A)$, guides the evolution of the Markov chain. In addition, we impose the physical constraint that the root mean square of our mass predictions with respect to AME2012 data [27] is no larger than the root mean square of Duflo-Zuker mass predictions with respect to AME2012. We make predictions for the mass corrections to the Duflo-Zuker mass model with the following mass parameterization:

$$M(Z,N) = M_{DZ}(Z,N) + a_N e^{-(Z-C)^2/2f} \qquad (2)$$

TABLE I. CPT mass results from this work showing cyclotron frequency ratios (r) and mass excess values. A comparison with the masses from the 2016 Atomic Mass Evaluation [49] is made. The # symbol indicates that these values are based solely on extrapolation.

				Mass excess of neutral atom [keV]		
Ion	Campaign	Reference ion	$r = [\nu_c(\text{ref})/\nu_c]$	CPT	AME2016	Δ(CPT-AME2016)
$^{154}Nd^{2+}$	IV	$^{82}Kr^+$	0.939 586 066 7(66)	−65579.6(1.0)	−65820(50)	241(51)
$^{156}Nd^{2+}$	IV	$^{82}Kr^+$	0.951 829 389 4(87)	−60202.1(1.3)	−60470(200)	267(200)
$^{158}Nd^{2+}$	IV	$^{84}Kr^+$	0.941 123 358 2(83)	−53835.1(1.3)	−54060(200#)	225(200#)
$^{159}Nd^{2+}$	I	$^{133}Cs^+$	0.597 967 11(12)	−49724(30)	−49810(300#)	86(300#)
$^{160}Nd^{2+}$	II	$^{84}Kr^+$	0.953 086 24(30)	−46725(47)	−47130(300#)	405(300#)
$^{162}Sm^{2+}$	III	$^{84}Kr^+$	0.964 954 683(32)	−54377.0(5.0)	−54530(200#)	153(200#)
$^{163}Sm^{2+}$	III	$^{84}Kr^+$	0.970 937 545(47)	−50599.6(7.3)	−50720(300#)	120(300#)
$^{164}Sm^{2+}$	III	$^{84}Kr^+$	0.976 913 350(26)	−47925.3(4.0)	−48100(300#)	175(300#)

for the hundreds of nuclear masses in the rare-earth region. We set $C = 60$ based on numerous preliminary runs in which this quantity consistently floated to this value and set $f = 10$ to ensure only local features in the mass surface are produced to avoid modifying mass trends near stability. We model 28 a_N parameters for $N = 93$–120. Although we consistently find $N < 109$ to dominate peak formation, we choose to allow $N = 109$–120 to float in order to prevent any edge effects from influencing our results in the peak region of $A \sim 159$–169. Updates to separation energies, Q values, β-decay rates, and neutron-capture rates for the roughly 300 nuclei in the region are performed at each time step in order to calculate the abundance prediction in a self-consistent manner [53]. This procedure leads to highly correlated parameters which cause a long integrated autocorrelation time and slow convergence. To explore the full parameter space, we make use of the parallel chains MCMC method. Our statistics were determined by considering the lowest χ^2 configuration (best step) of 50 independent, parallel MCMC runs. The calculation begins from Duflo-Zuker masses with an abundance pattern fit giving a $\chi^2 = 200$, and each run is allowed to explore the parameter space for 10 000–20 000 steps. As our parameters evolve away from zero, many solutions with $28 < \chi^2 < 200$ are readily found, but solutions with $\chi^2 \leq 28$ (as are the best steps of all runs) are more unique.

Initial runs located a number of solutions with an inversion of the odd-even behavior in one-neutron separation energies (S_n). We considered this to be an unphysical mechanism of peak formation and so discarded all such solutions. For subsequent runs, we introduced a veto in the algorithm, so it cannot explore mass surfaces with this reversal. This was implemented by requiring that the neutron pairing metric $D_n(Z,A) = (-1)^{A-Z+1}[S_n(Z,A+1) - S_n(Z,A)]$ remains positive. The result shown in Fig. 2 as the red band was determined by the average and standard deviation of 50 such runs, which have an average $\chi^2 \sim 23$. The dip in the red band mass surface of Fig. 2 at $N = 104$ produces an upward kink in the separation energy surface where the material, which eventually forms the peak, accumulates as the r-process path moves toward stability. In future work, we expect to be able to subdivide these runs by the details of the peak formation mechanism.

In Fig. 3, we estimate the role of differing thermodynamic conditions, by taking the average mass values from the red band in Fig. 2 and running this solution through the reaction network with a variety of similar astrophysical conditions. As can be seen from the figure, this produces relatively little variation in the abundance pattern.

The parameterization we used is able to find the trends in the mass surface needed for all nuclei which contribute to rare-earth peak formation; however, because relative differences in masses between isotopes are most relevant for peak formation, it allows only for the absolute scale of the neodymium ($Z = 60$) isotopic chain to be predicted by our MCMC procedure. Therefore, when we display our mass predictions for samarium in Fig. 2, we pin the predicted trend to AME2012 data. The black triangles in Fig. 2 show the newly measured masses for $^{154,156,158-160}$Nd and $^{162-164}$Sm determined by the CPT and listed in Table I. The local features in the mass surfaces predicted by our reverse-engineering analysis given the astrophysical

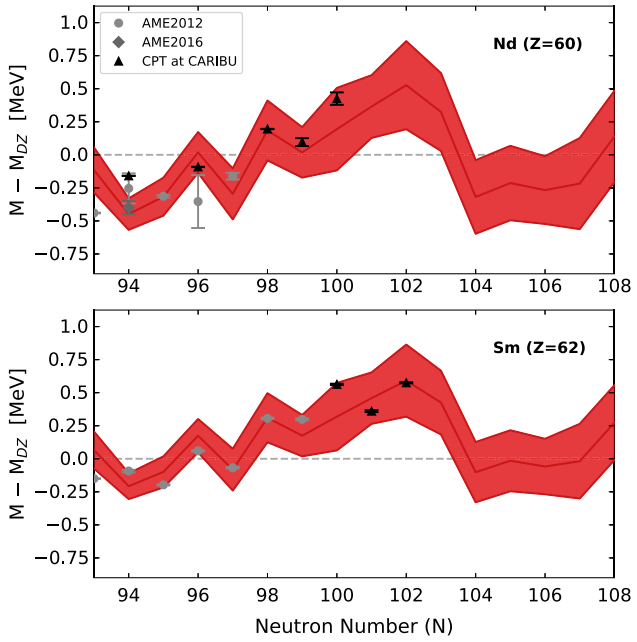

FIG. 2. Comparison between experimental values and theoretical predictions (red band) of the nuclear masses relative to the Duflo-Zuker mass model for neodymium and samarium isotopes in a merger accretion disk wind scenario ($s/k_B = 30$, $\tau = 70$ ms, and $Y_e = 0.2$).

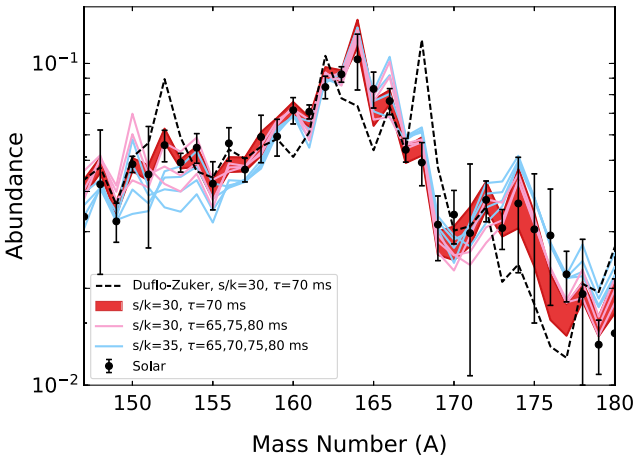

FIG. 3. Rare-earth peak abundances using Duflo-Zuker masses (black dashed line) as compared to the result for this same astrophysical trajectory after the algorithm finds the mass predictions in Fig. 2 (solid red band). Pink and blue curves serve to show the change in the abundance pattern obtained from using other disk wind parameters but with the same mass surface.

conditions of a neutron star merger wind scenario are consistent with the new precision mass measurements along both the neodymium and samarium isotopic chains.

In this Letter, we have reported the first direct mass measurements of eight neutron-rich neodymium and samarium isotopes, which are in good agreement with the mass surface trends which best reproduce the rare-earth peak abundance pattern in a hot, low entropy accretion disk wind scenario. We have highlighted the importance of precision experiments, such as the CPT mass spectrometer, in reducing the unknowns in nuclear properties which influence *r*-process events. Within a neutron star merger event, there are many trajectories describing distinct astrophysical conditions which are candidates to be the dominant *r*-process mechanism. Here we explored a hot, low-entropy accretion disk wind scenario, but there are other locations of interest such as the cold, neutron-rich tidal tail ejecta. Given the variety of astrophysical conditions capable of supporting an *r* process, it was not clear in advance that the masses compatible with this wind scenario would be consistent with the new experimental data. Since other astrophysical conditions can lead to different rare-earth peak formation mechanisms, additional theory calculations that span the range of possible *r*-process conditions must also be considered. The true test will come once the results from more extensive studies can be directly compared with measurements that are slightly more neutron rich. The collaborative approach between theory and experiment outlined in this Letter suggests that, with further progress, studies like this could make a definitive statement about the site (or sites) of the *r* process.

N. V. and R. S. thank Zoltán Toroczkai and Jorge Piekarewicz for useful discussions. This work was supported by the U.S. Department of Energy, Office of Nuclear Physics, under Contracts No. DE-AC02-06CH11357 (ANL) and No. PHY-1419765 (Nuclear Science Laboratory at the University of Notre Dame) and by NSERC (Canada), Application No. SAPPJ-2015-00034 (CPI 1199136). This research used resources of ANL's ATLAS facility, which is a DOE Office of Science User Facility. This work was supported in part by the U.S. Department of Energy under Contract No. DE-AC52-07NA27344 for the topical collaboration Fission In R-process Elements (FIRE). This work was also supported in part by the U.S. Department of Energy under Grants No. DE-SC0013039 (R. S.) and No. DE-FG02-02ER41216 (G. C. M.) and was enabled by the National Science Foundation under Grant No. PHY-1430152 (JINA Center for the Evolution of the Elements). A portion of this work was also carried out under the auspices of the National Nuclear Security Administration of the U.S. Department of Energy at Los Alamos National Laboratory under Contract No. DE-AC52-06NA25396 (M. R. M.). This work utilized the computational resources of the University of Notre Dame Center for Research Computing (ND CRC) and the Laboratory Computing Resource Center at Argonne National Laboratory (ANL LCRC). We specifically acknowledge the assistance of Scott Hampton (ND CRC) and Stanislav Sergienko (ANL LCRC).

Note added in proof.—The rare-earth region has also been recently studied by measurements at JYFLTRAP [54].

*rodney.orford@mail.mcgill.ca
†nvassh@nd.edu

[1] F. Hoyle, W. A. Fowler, G. R. Burbidge, and E. M. Burbidge, Science **124**, 611 (1956).
[2] E. M. Burbidge, G. R. Burbidge, W. A. Fowler, and F. Hoyle, Rev. Mod. Phys. **29**, 547 (1957).
[3] W. Hillebrandt, Space Sci. Rev. **21**, 639 (1978).
[4] J. J. Cowan, F.-K. Thielemann, and J. W. Truran, Phys. Rep. **208**, 267 (1991).
[5] M. Arnould, S. Goriely, and K. Takahashi, Phys. Rep. **450**, 97 (2007).
[6] C. Freiburghaus, S. Rosswog, and F.-K. Thielemann, Astrophys. J. Lett. **525**, 121 (1999).
[7] F.-K. Thielemann *et al.*, Prog. Part. Nucl. Phys. **66**, 346 (2011).
[8] National Research Council, *Connecting Quarks with the Cosmos: Eleven Science Questions for the New Century* (The National Academies Press, Washington, DC, 2003).
[9] B. P. Abbott *et al.* (LIGO Scientific Collaboration and Virgo Collaboration), Phys. Rev. Lett. **119**, 161101 (2017).
[10] P. S. Cowperthwaite *et al.*, Astrophys. J. Lett. **848**, L17 (2017).
[11] J. Wu *et al.*, Phys. Rev. Lett. **118**, 072701 (2017).
[12] S. N. Liddick *et al.*, Phys. Rev. Lett. **116**, 242502 (2016).
[13] J. A. Cizewski, A. Ratkiewicz, J. E. Escher, A. Lepailleur, S. D. Pain, and G. Potel, Eur. Phys. J. Web Conf. **165**, 01013 (2018).
[14] B. Côté *et al.*, Astrophys. J. **855**, 99 (2018).
[15] J. Barnes, D. Kasen, M.-R. Wu, and G. Martínez-Pinedo, Astrophys. J. **829**, 110 (2016).
[16] M. R. Mumpower, R. Surman, G. C. McLaughlin, and A. Aprahamian, Prog. Part. Nucl. Phys. **86**, 86 (2016).
[17] R. Surman, J. Engel, J. R. Bennett, and B. S. Meyer, Phys. Rev. Lett. **79**, 1809 (1997).
[18] M. R. Mumpower, G. C. McLaughlin, and R. Surman, Phys. Rev. C **85**, 045801 (2012).
[19] S. Goriely, J.-L. Sida, J.-F. Lemaître, S. Panebianco, N. Dubray, S. Hilaire, A. Bauswein, and H.-T. Janka, Phys. Rev. Lett. **111**, 242502 (2013).
[20] R. Surman, G. C. McLaughlin, M. Ruffert, H.-T. Janka, and W. R. Hix, Astrophys. J. **679**, L117 (2008).
[21] A. Perego, S. Rosswog, R. M. Cabezón, O. Korobkin, R. Käppeli, A. Arcones, and M. Liebendörfer, Mon. Not. R. Astron. Soc. **443**, 3134 (2014).
[22] S. Wanajo, Y. Sekiguchi, N. Nishimura, K. Kiuchi, K. Kyutoku, and M. Shibata, Astrophys. J. **789**, L39 (2014).
[23] O. Just, A. Bauswein, R. A. Pulpillo, S. Goriely, and H.-T. Janka, Mon. Not. R. Astron. Soc. **448**, 541 (2015).
[24] R. Fernández, D. Kasen, B. D. Metzger, and E. Quataert, Mon. Not. R. Astron. Soc. **446**, 750 (2015).
[25] A. Malkus, G. C. McLaughlin, and R. Surman, Phys. Rev. D **93**, 045021 (2016).

[26] J. Duflo and A. P. Zuker, Phys. Rev. C **52**, R23 (1995).
[27] M. Wang, G. Audi, A. H. Wapstra, F. G. Kondev, M. MacCormick, X. Xu, and B. Pfeiffer, Chin. Phys. C **36**, 1603 (2012).
[28] G. Audi, F. G. Kondev, M. Wang, W. J. Huang, and S. Naimi, Chin. Phys. C **41**, 030001 (2017).
[29] M. R. Mumpower, G. C. McLaughlin, R. Surman, and A. W. Steiner, Astrophys. J **833**, 282 (2016).
[30] M. R. Mumpower, G. C. McLaughlin, R. Surman, and A. W. Steiner, J. Phys. G **44**, 034003 (2017).
[31] S. Goriely, Astron. Astrophys. **342**, 881 (1999).
[32] H. Palme and H. Beer, in *Landolt Börnstein, New Series, Group VI* (Springer, Berlin, 1993), Vol. 3, p. 196.
[33] G. Savard, S. Baker, C. Davids, A. Levand, E. Moore, R. Pardo, R. Vondrasek, B. Zabransky, and G. Zinkann, Nucl. Instrum. Methods Phys. Res., Sect. B **266**, 4086 (2008).
[34] J. Van Schelt, D. Lascar, G. Savard, J. A. Clark, P. F. Bertone, S. Caldwell, A. Chaudhuri, A. F. Levand, G. Li, G. E. Morgan, R. Orford, R. E. Segel, K. S. Sharma, and M. G. Sternberg, Phys. Rev. Lett. **111**, 061102 (2013).
[35] T. Y. Hirsh *et al.*, Nucl. Instrum. Methods Phys. Res., Sect. B **376**, 229 (2016).
[36] R. N. Wolf, G. Marx, M. Rosenbusch, and L. Schweikhard, Int. J. Mass Spectrom. **313**, 8 (2012).
[37] N. E. Bradbury and R. A. Nielsen, Phys. Rev. **49**, 388 (1936).
[38] S. Eliseev, K. Blaum, M. Block, C. Droese, M. Goncharov, E. M. Ramirez, D. A. Nesterenko, Y. N. Novikov, and L. Schweikhard, Phys. Rev. Lett. **110**, 082501 (2013).
[39] M. König, G. Bollen, H.-J. Kluge, T. Otto, and J. Szerypo, Int. J. Mass Spectrom. **142**, 95 (1995).
[40] G. Savard *et al.*, Int. J. Mass Spectrom. **251**, 252 (2006).
[41] J. Van Schelt, D. Lascar, G. Savard, J. A. Clark, S. Caldwell, A. Chaudhuri, J. Fallis, J. P. Greene, A. F. Levand, G. Li, K. S. Sharma, M. G. Sternberg, T. Sun, and B. J. Zabransky, Phys. Rev. C **85**, 045805 (2012).
[42] S. Eliseev *et al.*, Appl. Phys. B **114**, 107 (2014).
[43] G. Bollen, H.-J. Kluge, M. König, T. Otto, G. Savard, H. Stolzenberg, R. B. Moore, G. Rouleau, G. Audi, and ISOLDE Collaboration, Phys. Rev. C **46**, R2140 (1992).
[44] G. Audi, F. G. Kondev, M. Wang, B. Pfeiffer, X. Sun, J. Blachot, and M. MacCormick, Chin. Phys. C **36**, 1157 (2012).
[45] T. R. England and B. F. Rider, Report No. LA-UR-94-3106 ENDF-349, Los Alamos National Laboratory, 1995.
[46] R. C. Greenwood and M. H. Putnam, Nucl. Instrum. Methods Phys. Res., Sect. A **337**, 106 (1993).
[47] *Proceedings of the Conference on Exotic Nuclei and Atomic Masses ENAM-2001*, 1st ed. (Springer-Verlag, Berlin, 2003), p. 479.
[48] P. C. Sood, R. Gowrishankar, and K. Vijay Sai, J. Phys. G **39**, 095107 (2012).
[49] M. Wang, G. Audi, F. G. Kondev, W. J. Huang, S. Naimi, and X. Xu, Chin. Phys. C **41**, 030003 (2017).
[50] B. D. Metzger, T. A. Thompson, and E. Quataert, Astrophys. J. **676**, 1130 (2008).
[51] S. Wanajo, Y. Sekiguchi, N. Nishimura, K. Kiuchi, K. Kyutoku, and M. Shibata, Astrophys. J. **789**, L39 (2014).
[52] A. Perego, S. Rosswog, R. M. Cabezón, O. Korobkin, R. Käppeli, A. Arcones, and M. Liebendörfer, Mon. Not. R. Astron. Soc. **443**, 3134 (2014).
[53] M. R. Mumpower, R. Surman, D.-L. Fang, M. Beard, P. Möller, T. Kawano, and A. Aprahamian, Phys. Rev. C **92**, 035807 (2015).
[54] M. Vilen *et al.*, preceding Letter, Phys. Rev. Lett. **120**, 262701 (2018).